**Article:**
Al-Tameemi, H.A., Long, H. orcid.org/0000-0003-1673-1193 and Dwyer-Joyce, R.S. (2018) Initiation of sub-surface micro-cracks and white etching areas from debonding at non-metallic inclusions in wind turbine gearbox bearing. Wear, 406-407. pp. 22-32. ISSN 0043-1648

https://doi.org/10.1016/j.wear.2018.03.008

# Initiation of sub-surface micro-cracks and white etching areas from debonding at non-metallic inclusions in wind turbine gearbox bearing

H.A. Al-Tameemi, H. Long, R.S. Dwyer-Joyce

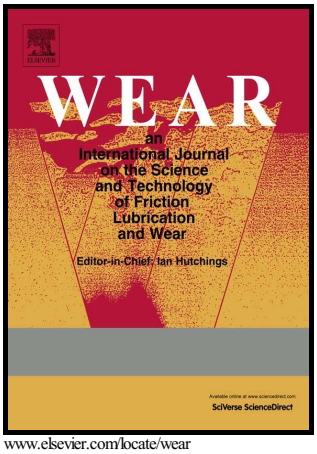


www.elsevier.com/locate/wear

PII: S0043-1648(18)30052-8
DOI: https://doi.org/10.1016/j.wear.2018.03.008
Reference: WEA102378

To appear in: *Wear*

Received date: 8 January 2018
Revised date: 20 February 2018
Accepted date: 18 March 2018

Cite this article as: H.A. Al-Tameemi, H. Long and R.S. Dwyer-Joyce, Initiation of sub-surface micro-cracks and white etching areas from debonding at non-metallic inclusions in wind turbine gearbox bearing, *Wear,* https://doi.org/10.1016/j.wear.2018.03.008

# Initiation of sub-surface micro-cracks and white etching areas from debonding at non-metallic inclusions in wind turbine gearbox bearing

H. A. Al-Tameemi, H. Long*, R. S. Dwyer-Joyce

Department of Mechanical Engineering, The University of Sheffield, Sheffield, S1 3JD, UK

*Corresponding author. Dr Hui Long, h.long@sheffield.ac.uk

## Abstract

In this study, a failed planetary bearing from a wind turbine gearbox was destructively examined to investigate the initiation of micro-cracks and butterflies at non-metallic inclusions, and the effect of debonding between these inclusions and the steel matrix. The butterflies were scanned using Atomic Force Microscopy (AFM) to show the topography that could not be assessed by using other microscopy techniques. Nano-indentation was conducted across a butterfly wing and a non-metallic inclusion to measure the hardness at the interface with the steel matrix. It was found that the White Etching Areas (WEA) in the region of the butterfly wing was a damaged material that showed tearing at the debonding gap between the inclusion and steel matrix. This study highlighted the effect of debonding on the initiation of micro-cracks, WEA and inclusion cracking. A direct relationship was found between the size of inclusions and the total length of inclusions and micro-cracks or butterfly wings. The depth of the observed sub-surface damage was correlated with the sub-surface stress distribution and these results suggested that surface traction could be an important contributing factor to the subsurface damage initiation.

**Keywords**: white etching cracks; white etching areas; non-metallic inclusions; rolling contact fatigue; surface traction.



## 1 Introduction

The premature failure of Wind Turbine Gearbox (WTG) bearings has been reported to be mainly resulted from White Etching Cracks (WECs) and research currently continues to uncover their root causes. The White Etching Areas (WEAs) initiated from non-metallic inclusions and formation of 'butterfly wings' were reported to be related to the WECs. The most common mode of premature failure is due to WECs which cause pieces of material to flake away from the surface (White Structure Flacking (WSF)) [1][2][3]. The damage may be initiated from the surface or sub-surface in bearing raceways [3][4][5]. The surface initiation hypothesis suggests that cracks could be caused by surface flaws and worsened by loading

conditions [3][6][7][8]. On the other hand, material defects such as non-metallic inclusions located in the sub-surface could serve as damage initiators [9][10][11]. Other damage initiation hypotheses have been proposed, including the effect of hydrogen, plastic deformation, and unconsidered loadings such as impact load causing lubrication film to breakdown [12][13][14][15][16]. In addition, a recent study highlighted the combined effect of material defects of non-metallic inclusions and tensile stress due to bearing seat waviness on the subsurface initiation of axial cracking and WECs formation [17]. However, a clear explanation of damage initiation, such as WECs surrounded by WEAs, and their root causes, i.e. abnormal loads during transient operation events, has not been established.

The WEA can be seen using optical microscopy after etching with nital (~ 2% nitric acid in ethanol) or picral [2][13][14]. The microstructure changes shown in premature bearing failure due to WSF are not uniform in shape or distribution which is why they are named as irregular White Etching Areas (irWEA) [12][18]. The microstructure of a WEA is nano-recrystallized, carbide-free ferrite grains in size ranging from 10 to 100 nm, supersaturated with carbon [19][20]. A number of factors have been reported to affect the initiation of WEC/WEA, such as the influence of non-metallic inclusions [11][19][21][22], the amount of retained austenite [5], the type of lubricant used in the operation and consequently the amount of hydrogen generated [6][23], as well as the level of Hertzian contact stress induced by loading [10][22]. When the WEAs form around an inclusion or a void, the microscopy observation in two dimensions shows butterfly wings being decorated with the WEAs. The sub-surface micro-structure changes in WEAs are thought to be related to the WECs, initiated by micro-cracks associated with the butterflies, which then propagate to the surface to cause WSF [11][17][19].

Previous work was conducted through destructive investigations of a failed sub-megawatt WT gearbox planetary bearing in which Manganese Sulphide (MnS) inclusions were identified as the main cause of sub-surface damage initiation [11]. This current study focusses on sub-surface damage initiation from non-perfectly bonded inclusions to the steel matrix to investigate the effect of surface traction on the initiation of sub-surface damage caused by these inclusions. The characteristics of the damaged inclusions and micro-cracks are analysed and correlated with the levels of sub-surface stresses. Atomic Force Microscopy (AFM) analysis is utilised in order to characterize the debonding separating the MnS inclusion from the steel matrix and the butterfly wings around the inclusion. More than 150 inclusions were analyses and relationships between the characteristics of the subsurface initiated damage and the initiating inclusions were found.

## 2 Examination procedure

The bearing under investigation was a single row Cylindrical Roller Bearing (CRB) used in the planetary gears of a three-stage wind turbine (WT) gearbox. This through hardened bearing was used in an on-shore WT with a 600 kW power rating. The bearing was in service for five years before out of service after a site inspection which found abnormal noise during

operation. The visual inspection showed extreme surface damage on the inner raceway compared to the outer raceway. The damaged area was in the loaded-zone where a unidirectional load was applied in the planetary bearing, as shown in Figure 1.

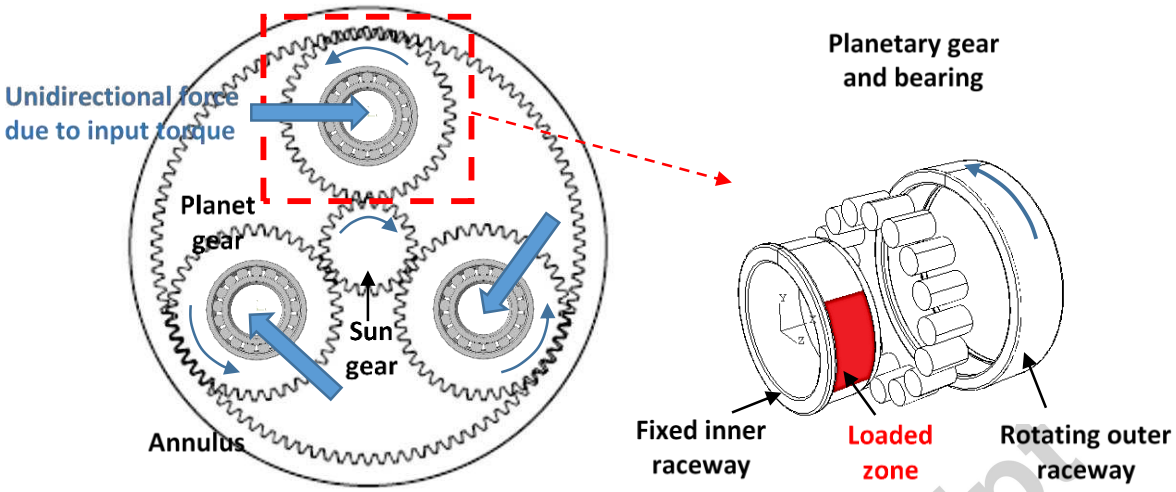


**Fig 1: Illustration of WT planetary gear stage showing the unidirectional load and the loaded zone on the inner raceway of the planetary bearings**

The dimensions of the examined inner raceway were 65mm in inner radius, 47 mm in raceway width, and 12.5 mm in thickness. Only half of the inner raceway of the failed bearing was available for examination in this study, and the results obtained refer only to this half of this bearing, while the other half was used for another study [11]. Three regions of damage can be identified on the surface of the bearing, as shown in Figure 2. The first region consisted of big spalls, bigger than 3 mm as the maximum dimension, spreading on the downwind side of the raceway. The width of this region was about 20 mm. At the entrance to the loaded zone, less spalling damage was observed with the largest spalls in this region located on the flange side. The red dotted line in Figure 2 shows the wear trace line which was not parallel to the axial axis of the raceway. This could be due to skewing of the rollers when entering to the loaded zone. Outside these two regions, no visual damage was observed however an optical microscopic examination of the surface showed some micro-indents.

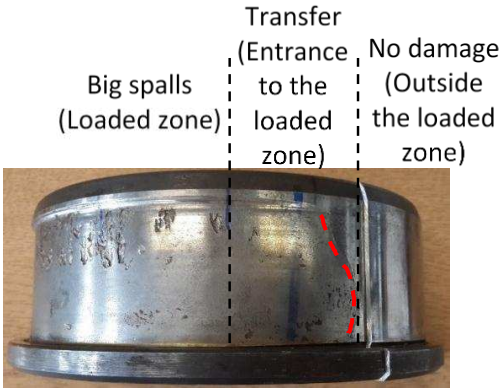


**Fig 2: Inner raceway of the examined failed bearing**

The inner raceway was destructively investigated by cutting and preparing samples in the axial and circumferential directions for microscopic examination. Various sections at different locations of the bearing inner raceway were cut to include the severely damaged surface, the slightly damaged surface and the visually non-damaged surface. After grinding and polishing, the samples were etched with 2% nital to reveal the microstructure changes of WEA in butterflies and WECs. The examination of the sub-surface using optical microscopy and Scanning Electron Microscopy (SEM) covered more than 1 mm depth from the surface. Further characterization of the debonding of the inclusions from the steel matrix and the chemical elements of the inclusions were also carried out using Energy Dispersive X-ray spectroscopy (EDX).

To obtain detailed mapping images of some of the butterflies, Atomic Force Microscopy (AFM) was used to provide measurements of the topography of the surface of the WEA at the nano-scale. In addition, AFM was utilized to clearly show the separation of the debonded MnS inclusions from the steel matrix. The images obtained helped in characterising the gaps attached to the MnS inclusions and the WEAs. The AFM revealed more details on the deformations in the WEA as shown in Figure 3 that could not be revealed by the optical microscope or the SEM, which are limited by two dimensional images.

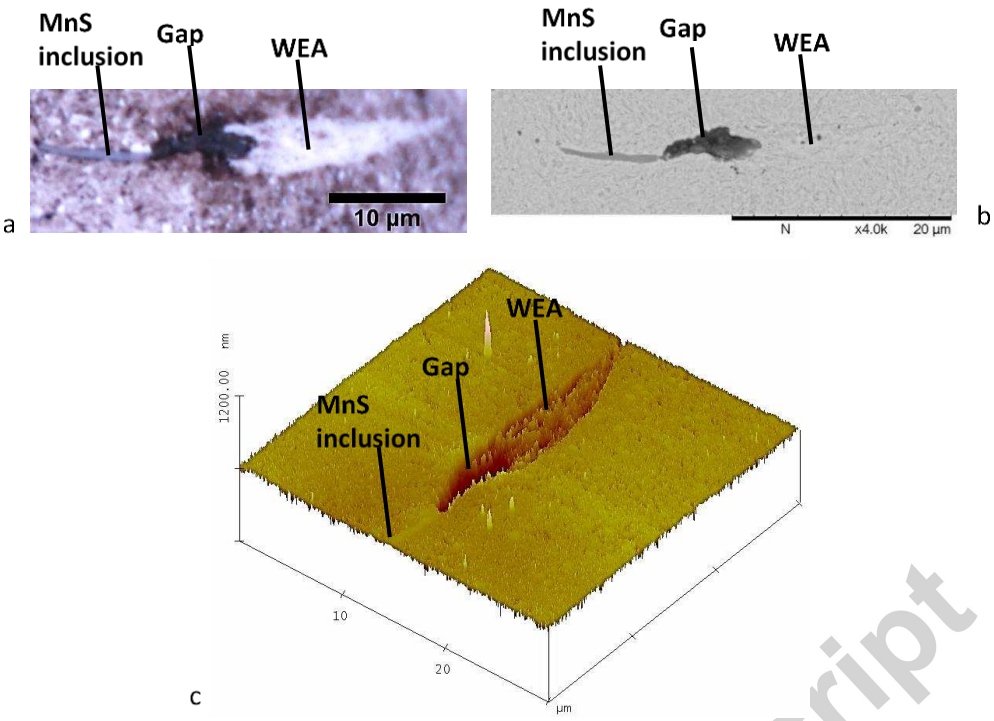


**Fig 3: Illustration of the difference between images of the same feature taken by different microscopic techniques (a) optical microscopic (b) SEM (c) AFM**

Micro and Nano-indentation were used to measure the hardness of the bearing steel, inclusions and microstructure alteration of WEA (butterflies), and to correlate the measurements with the damage initiation. To identify the depth of maximum hardness under the surface, the variation in hardness under the surface was measured using a Struers Micro/Macro Hardness tester (DuraScan). The Vickers hardness test was conducted with a load of 0.3 kgf and a holding time of 15 seconds. The adopted pattern of indentation was a vertical matrix of 6×3 indents with the first row positioned at 70 µm from the contact surface, and the distance between the centre of the indents in the horizontal and vertical direction was 100 µm. Then, the mean value and the standard deviation were calculated for indents at the same depth. To measure the hardness of a MnS inclusion and a butterfly wing, a Nano-indentation was conducted. This measurement also helped to identify the hardness of the interface region between a butterfly wing and the steel matrix. The test was carried out with a single loading-unloading step for each indent using a Hysitron Triboscope Nano-mechanical test system attached to a Bruker Dimension 3100 AFM. The pattern of indentation is presented with the measurements in Section 4.3.

## 3 Characterization of Inclusions and Damage

This study aimed to identify the initiation of damage that eventually caused the premature failure in the bearing. Initiation was defined as the appearance of a discontinuity in the material (steel matrix or inclusions) in the form of cracks of few microns to a few millimetres in length, or micro-structure alterations in the form of WEAs. The definitions of all the types

of damage observed during the examination of the failed bearing are presented in Table 1. It should be noted that more than one type of damage could be observed at the same time such as debonding and cracked inclusions. Figure 4 shows examples of different types of damage defined in Table 1. A database of the damage was created by recording the length, angle and depth for cracks, inclusions and WEA in the axial and circumferential sections. Figure 5 depicts the procedure adopted to measure the angle of inclusion and the butterfly wings. This figure shows the right and left wings of the butterfly, which are defined relatively to the Over Rolling Direction (ORD). The same definition for the angle was applied to the right and left cracks initiated from an inclusion. The length of the inclusion represented the distance between the two pointed tips, or the radius for globular inclusions, and the width was the maximum dimension normal to the length. The depth was measured from the surface to the centre of the inclusion.

**Table 1: Definitions of the damage observed and investigated**

| Damage Type | Definition |
|---|---|
| Inclusions initiated damage | Inclusion cracked or debonded from the steel matrix by a gap or non-perfect bonding; inclusion initiated cracks into the matrix or inclusion formed WEA; or inclusion linked to any surface or subsurface initiated crack or WEC. |
| Debonded inclusion | Inclusion not perfectly bonded with the steel matrix, a line of debonding can be seen in the interface, or a gap separating part of the inclusion from the steel matrix. |
| Cracked inclusion | Inclusion that has one or more micro-cracks across itself which may or may not extend to the steel matrix. |
| Micro-crack initiated by inclusions | Crack initiated from an inclusion, which could be debonded, and propagating into the steel matrix. It may or may not attach to WEA (butterfly wing). |
| WEA | A microstructure change which appears white under optical microscopy and shows dissolution of the spherical carbide which are normally observed in the martensitic bearing steel. The WEA could be observed around an inclusion or a void to form a butterfly or along a crack to form WEC. |
| Butterflies | Inclusion with one or two wing(s) of WEA, with or without micro-crack(s) in the WEA. The wings have specific inclination angles relative to the surface, or the Over Rolling Direction (ORD). |
| WECs | Single crack or network of cracks which is normally longer than the total length of a butterfly (inclusion + wing(s)) with WEA along the whole or part of the crack or network of cracks. The WECs could be connected to the surface of contact or completely under the surface with no specific inclination angle. The WECs could be linked to inclusion(s). |

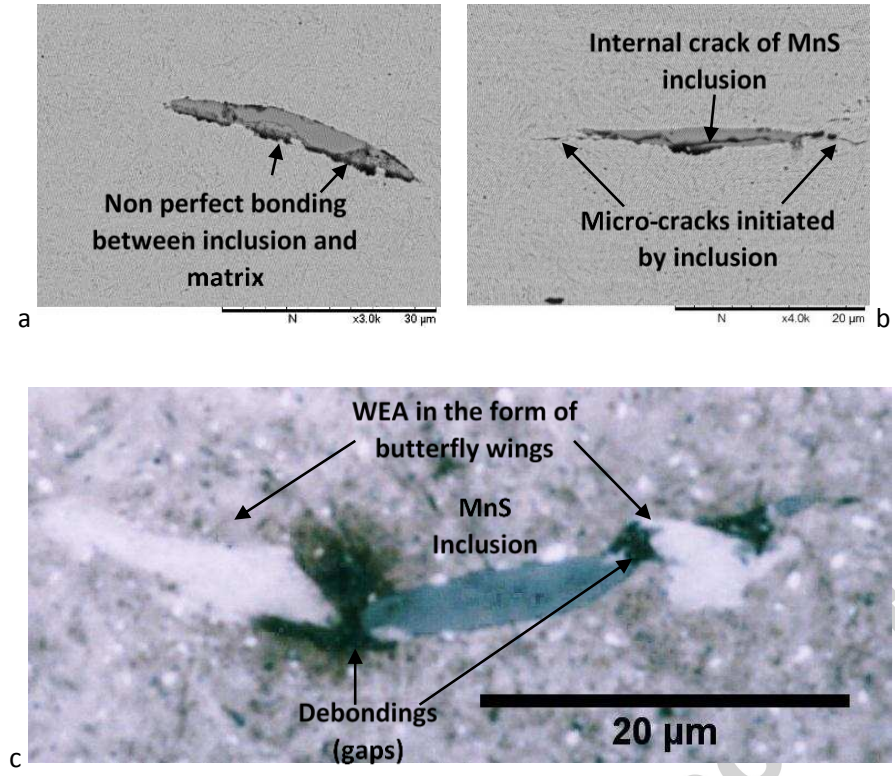


**Fig 4: Examples for the damage defined in Table 1 (a) Debonded inclusion (b) Cracked inclusion with micro-cracks (c) Butterfly with WEAs debonded from matrix**

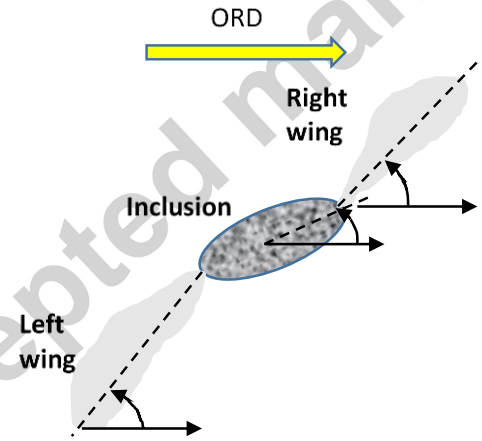


**Fig 5: Definition of the angles of inclusion and butterfly right and left wings**

## 4 Specifications of inclusions initiated damage

The prepared samples were scanned for characterising the types of damage defined in Table1. The emphasis here was on identifying the sub-surface damage initiators, namely inclusions initiated damage. Four types of inclusions were logged and they are defined as: debonded inclusion, cracked inclusion, inclusion that initiated micro-cracks, and butterfly inclusion. The characteristics of these inclusions, and the associated micro-cracks or micro-

structure changes (WEA) were analysed. The most common inclusions found in this bearing were light grey elongated inclusions. Inclusions with these features are classified as Type A-Sulfide which could be manganese sulphides [24] or aluminates embedded in manganese sulphide according to the standards ASTM-E45-13 and ISO-4967 [25]. Determining the exact components of these inclusions was performed using energy dispersive x-ray (EDX) which revealed the presence of Manganese (Mn) and Sulphur (S) as shown in Figure 6.

## 4.1 AFM analysis of debonding and butterfly wings

The dark tips of some of the inclusions, which could be mistaken for encapsulated oxide, were identified using AFM and SEM as shown in Figure 7, and they were found to be discontinuities between the inclusion and the steel matrix as debondings (gaps). The debondings may have been manufacturing defects and evidence of this has been reported in manufacturing studies ([26][27][28]). In this study, debondings were observed at different depths from the surface, greater than 1 mm as shown in the right image in Figure 7. Sometime these debonded inclusions were found far from the zone of high sub-surface stress, which was calculated using the Hertzian contact theory. Accordingly, these debondings were mostly material defects rather than results of loading in operation. These deep inclusions were not included in the database of the catalogued inclusions which was used to identify the characters of inclusions initiated damage.

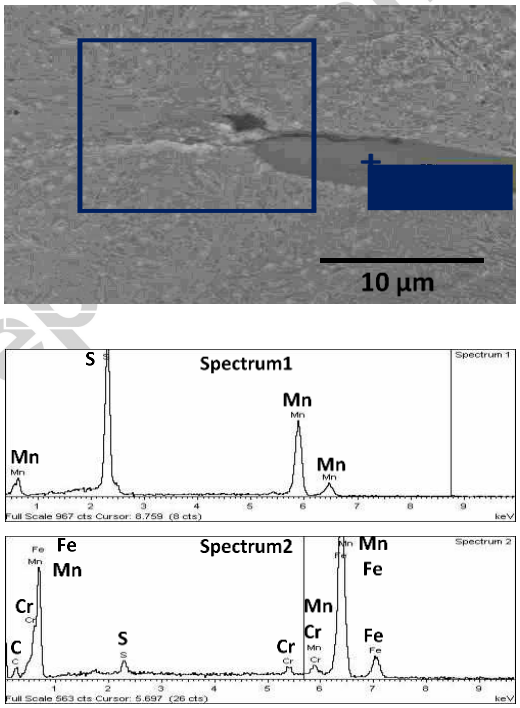


**Fig 6: EDX analysis (spectrum 1) point identification of a MnS inclusion and (spectrum 2) area identification of a WEA and inclusion**

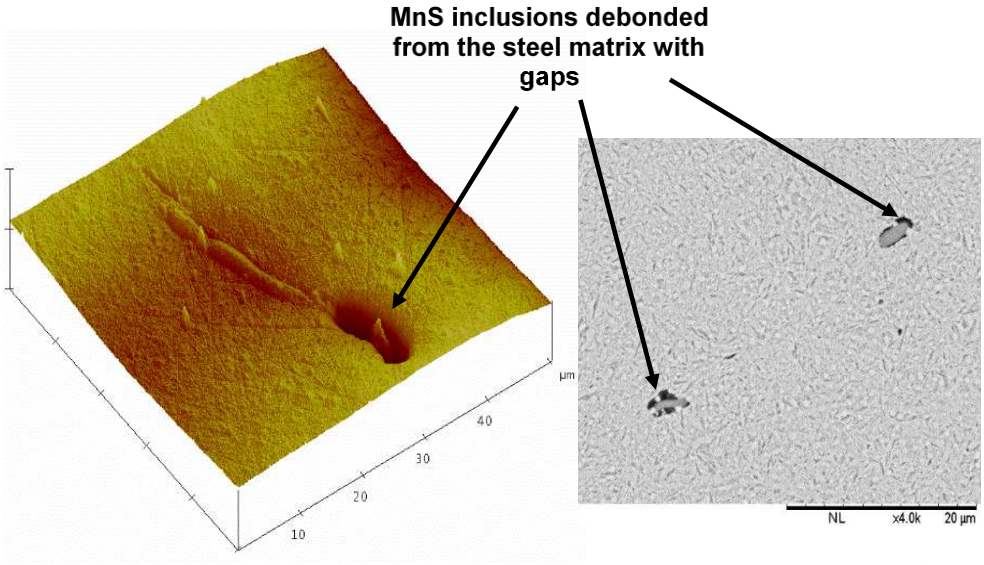


**Fig 7: (Left) AFM 3D image and (Right) SEM image of debonded inclusions at 1300 µm depth**

It was observed that WEAs in butterfly wings, were mostly attached to the debonding gaps at inclusion tips rather than the inclusions directly. This could be due to the higher stress concentration factor at debondings around the inclusion tips [29][30]. Debondings were found with different shapes around inclusions. To gain an insight on the size of the inclusion as well as examining the topography of the WEA, AFM analysis was conducted. The single wing butterfly shown in Figure 3 was examined using AFM. This butterfly was at 207 µm under the surface and it showed a MnS inclusion with a debonding gap at one of its tips, and a single butterfly wing was found to be attached to the debonding. After an AFM scan, the depth along two lines crossing the debonding was characterised as shown in Figure 8. The WEA was found to be lower than the steel matrix, and the discontinuity between the inclusion and the WEA was clearly shown by the relative depth. The maximum dimensions for this debonding were found to be 2.3 µm in depth, 9.6 µm in length and 3.3 µm in width. This analysis shows the extent of damage in the form of a material discontinuity starting from the debonding gap of the inclusion into the steel matrix in the form of WEA that has a degree of discontinuity and damaged material. The WEA is shown to be a microstructural change accompanied by damage to the material.

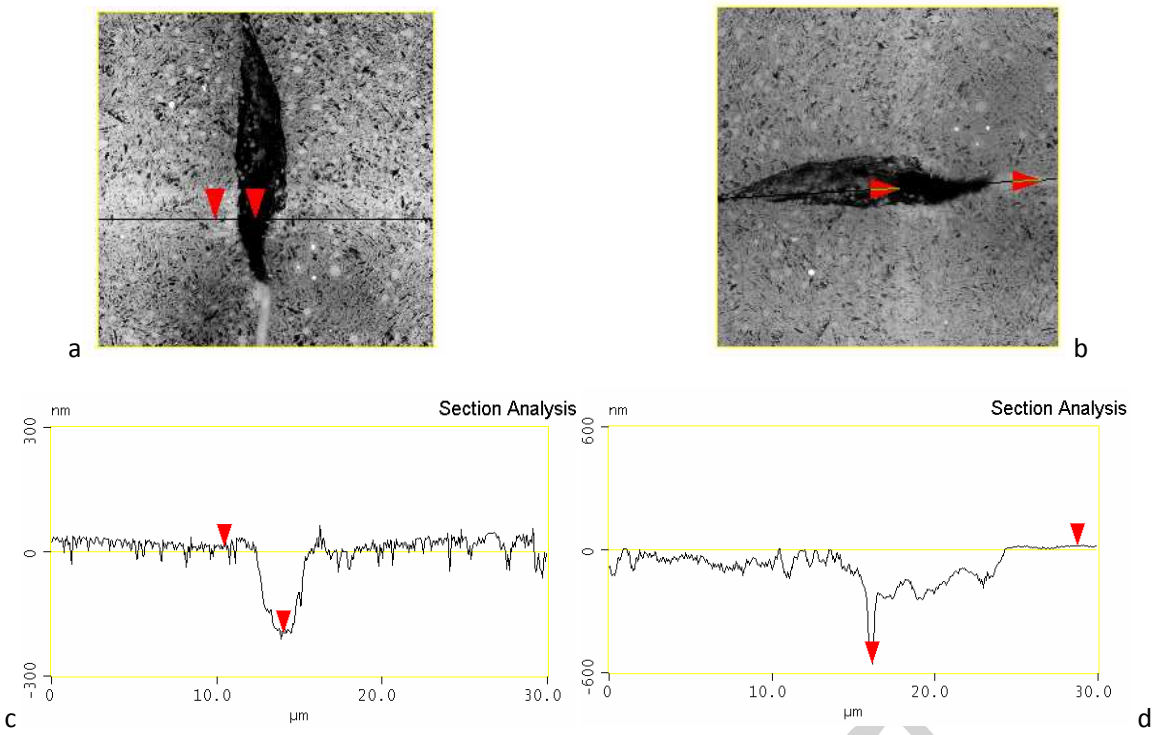


**Fig 8: AFM analysis showing the debonding between a MnS inclusion and WEA (butterfly wing)**

The AFM imaging measurements also showed that the WEA was not a dense material, and it resembled a damaged material extending from the debonding at the inclusion tip. Figure 9 shows three butterfly wings observed in the axial and circumferential sections with 3D AFM images for the WEAs. These images show clearly the features of the WEAs that are not available by 2D optical or SEM images. The borders of the WEA show a sudden transition from the dense steel matrix to the discontinuous material inside the WEA. This could be due to a local stress concentration that pulls or shears the edges of the WEA (i.e. the interface with the steel matrix). The hardness of the WEA was reported to be higher than the steel matrix [1], and this was confirmed in this investigation and results to be discussed in Section 4.3. This could be an indication of material hardening after the bearing steel yield limit had been exceeded due to stress concentration around the debonding of inclusion.

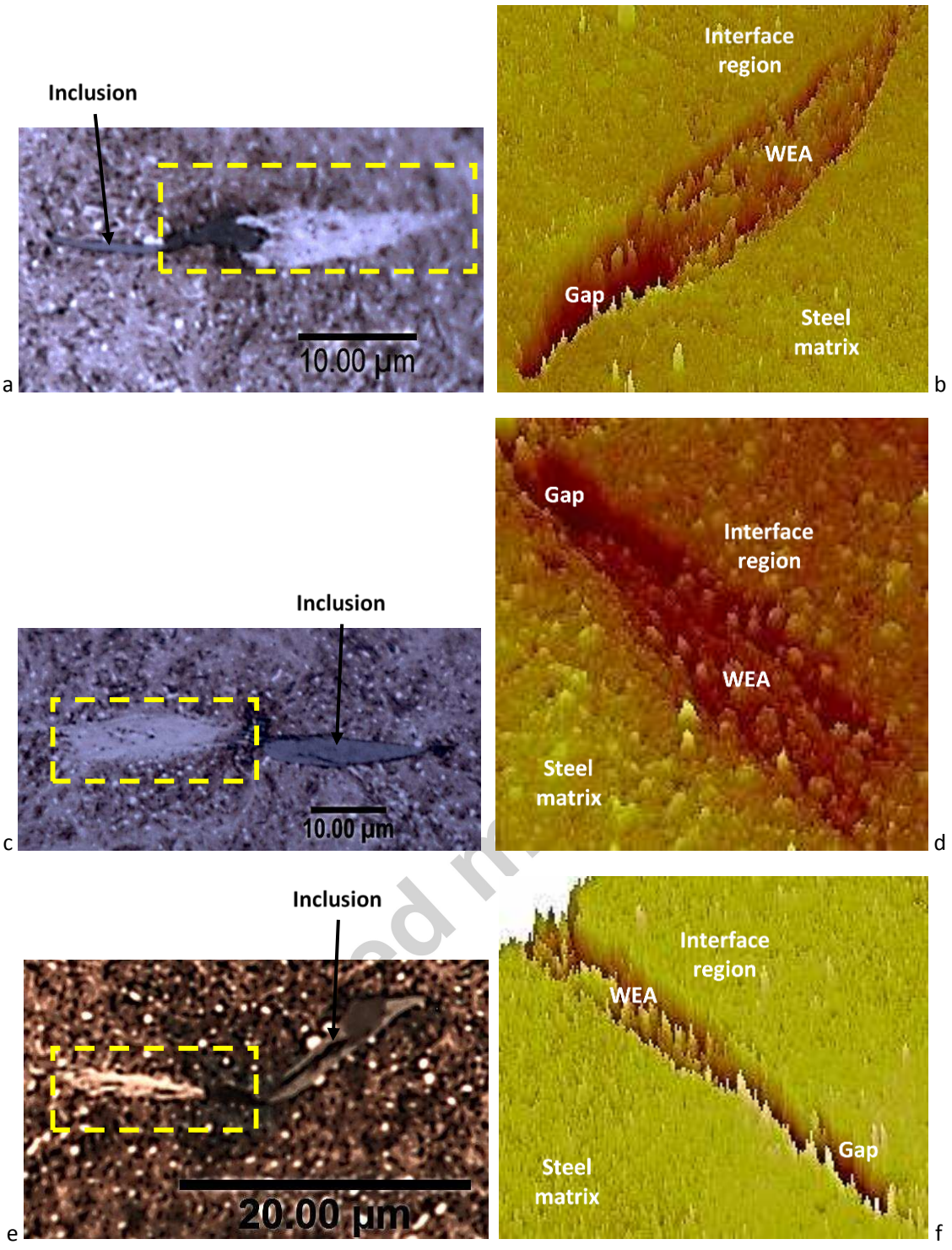


**Fig 9: (Left) Optical images of debonded MnS inclusions attached to WEA. The highlighted parts are the 3D AFM images to show the discontinuity of the WEA, and the debonding at the boundaries between the WEA and the steel matrix. The images in (a) to (d) are from axial sections; and (e) and (f) are from circumferential section with ORD from left to right**

### 4.2 Cracked inclusions and cracks initiated by inclusion

Some of the observed micro-cracks and WEA (butterfly wings) were initiated by inclusions with internal cracking as shown in Figure 10 (a) and (b). It was more likely that the micro-cracks started from the interface between the inclusion and the steel matrix, since no cracked inclusion was found where the internal crack does not interact with this interface. It was also observed that some micro-cracks propagated into the steel matrix or formed butterfly wings could initiate from the debonding between the inclusion and the steel matrix where the inclusions were not cracked themselves. An example of this was the non-cracked inclusion with debonding which formed a butterfly as shown in Figure 9 (a). In other cases, micro-cracks into the steel matrix were initiated from inclusions tips without debonding or inclusion internal cracking as shown in Figure 10 (c) and (d). Accordingly, no specific order for the damage initiation can be confirmed in this study.

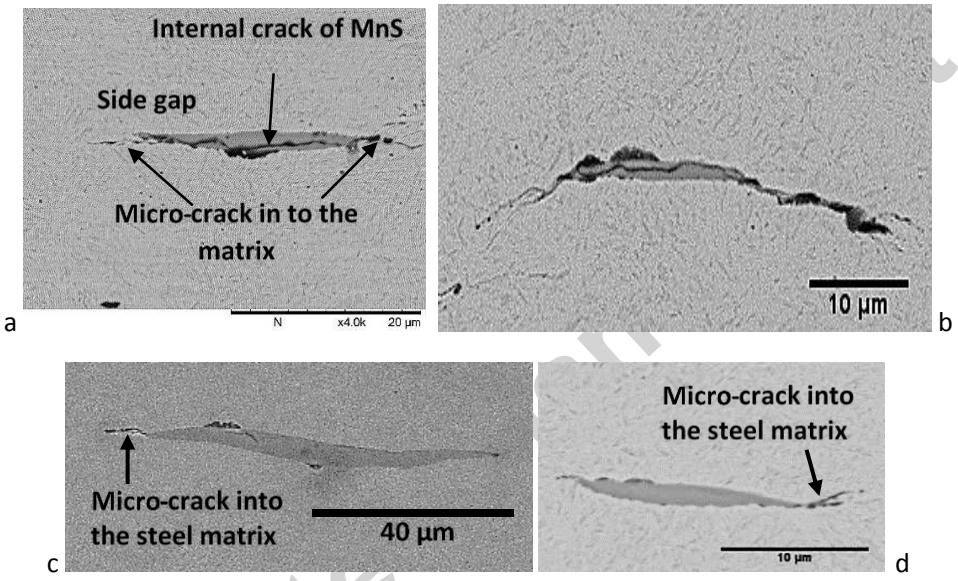


**Fig 10: Micro-cracks initiated by inclusions (a) and (b) cracked inclusions with cracks propagated into the steel matrix (c) and (d) Micro-cracks initiated from non-cracked inclusions**

In addition to the micro-cracks, one fully developed crack linking the surface with two butterflies was found as shown in Figure 11. In this figure, no inclusions could be found in the butterflies which may have been removed by the sample preparation process. Since no spalling damage was linked to the WEC, it appeared most likely that this crack propagated from the butterflies and it was not initiated from the surface. It also showed that cracks and WECs could initiate from the inclusions, or the interface between a WEA and the steel matrix. These cracks propagated in a vertical direction towards the surface or deeper down without following the extension direction of the butterfly wings and this suggested a different mechanism for the initiation and propagation.

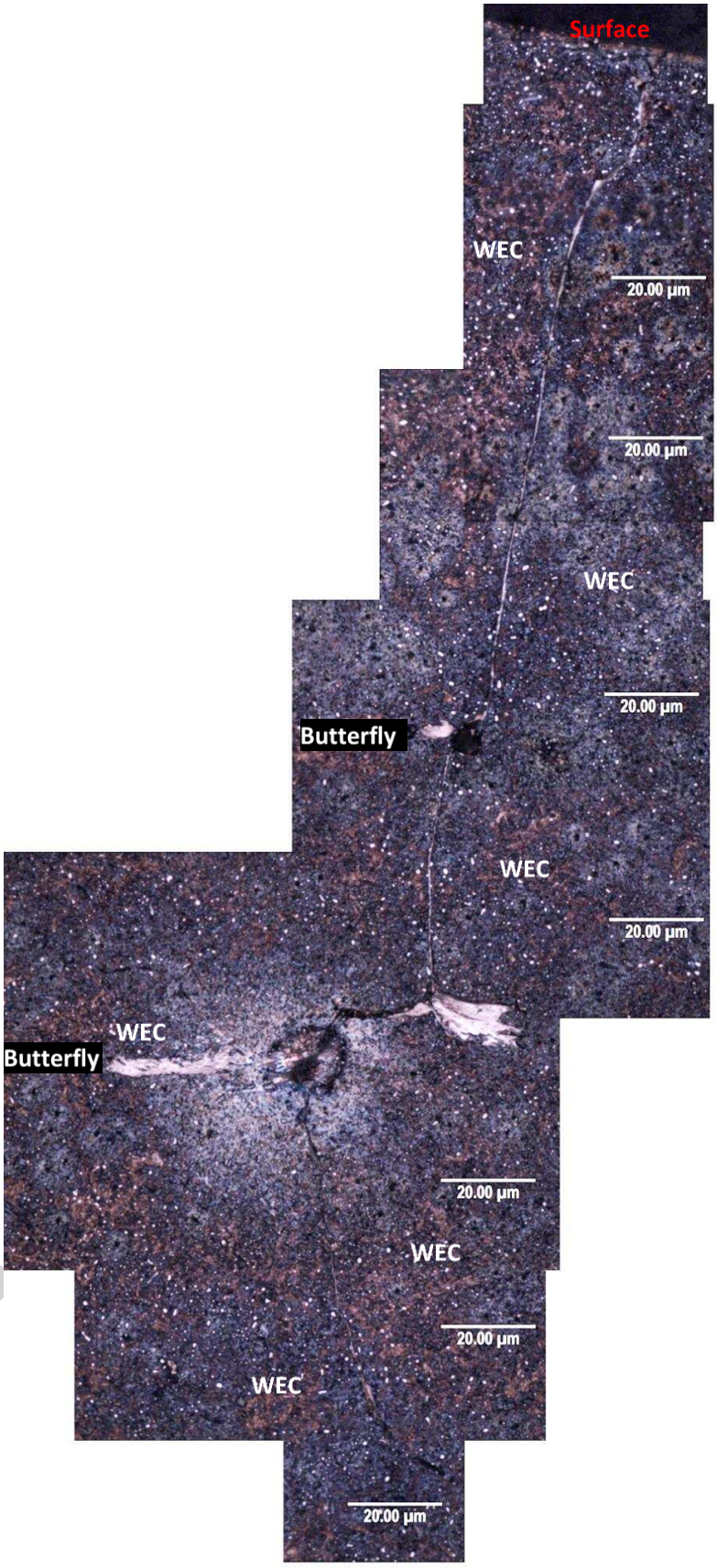


**Fig 11: WEC propagated almost vertically toward the surface and linked to two butterflies**

### 4.3 Hardness of MnS inclusion, WEA and the interface

The hardness of a MnS inclusion and a WEA in a butterfly was measured using Nano-indentation. The measurement applied to both the inclusion and the WEA of the butterfly in Figure 9 (c) which located 63 µm from the surface. The pattern of indents used was a line of 20 as shown in the AFM images in Figure 12. These arrays of indents across the MnS inclusion and the butterfly wing showed the indents as dark triangles above or below the numbers. A spacing of 0.5 µm between indents and load of 800 µN were used in the measurements. These values of load and spacing were decided after testing the indent's size, which was around 0.2 µm, to ensure sufficient spacing between the indents and having sufficient number of indents across the inclusion and the WEA width. The spacing of around 2.5 to 3 times of the size of the indents should eliminate the effect of localized plastic deformation at each indent on the adjacent indents [31]. It can be seen in Figure 12 that not all the indents had the same size, especially within the steel matrix and the WEA. Some of the variation in the measurements was related to the multi-phase nature of steel on the nano-scale which was also true for the WEA [32].

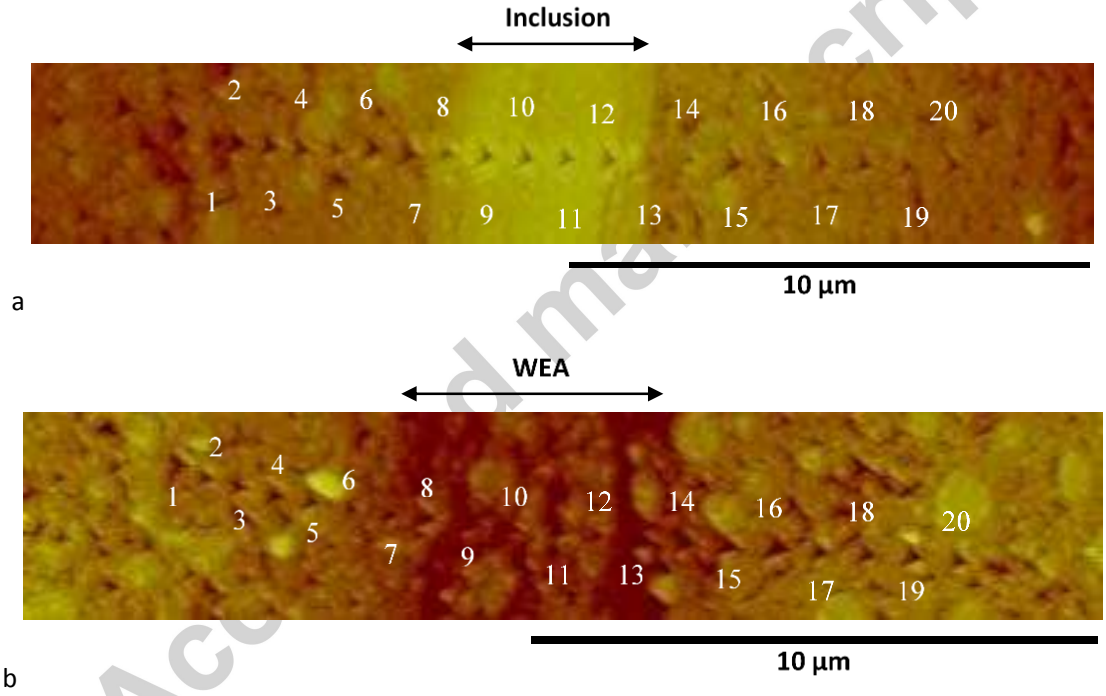


**Fig 12: Nano indents across (a) MnS inclusion and (b) butterfly wing in Figure 9 (c)**

The curve in Figure 13 shows the variation of hardness across the inclusion, and the WEA (butterfly wing) with the indent numbers referred to those in Figure 12. The results from the first and the sixth indents in the WEA-steel matrix curve, and the third and the fifteenth in the inclusion-steel matrix curve were excluded because they were clear outliers. As shown in Figure 13, at indents number 9 and 13, the lower hardness revealed the weak interface between the WEA and the steel matrix, which could justify the observed butterfly micro-cracks at the edges of the butterfly wing. Also, the WEA was generally observed at one of the sides of the WECs however there was no general conclusion regarding which specific side.

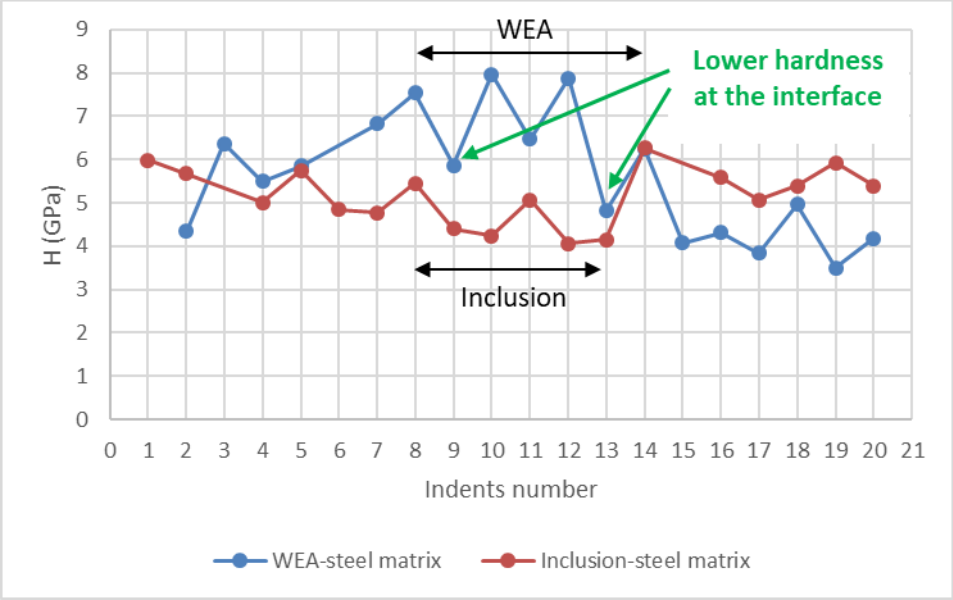


**Fig 13: Nano indentation hardness measurement across a MnS inclusion and a butterfly wing**

## 5 Statistical Analysis of Subsurface Damage

The inclusions observed consisted of the inclusions initiated damage and inclusions not initiated damage and these were catalogued according to the definitions given in Table 1. The selection of inclusions not initiated damage was random but they were selected from locations close to the inclusions initiated damage. In total 153 inclusions in the axial and circumferential sections were recorded, but some of them showed more than one type of damage, and were therefore classified in more than one damage category. The total number of analysed inclusions, both inclusions initiated damage and inclusions not initiated damage, was therefore 208. It was found that almost 60% of the debonded inclusions also exhibited one or more of the other three types of sub-surface initiated damage, namely cracked inclusions, micro-cracks initiated from inclusion and butterflies. For the micro-cracks initiated by inclusion, 52% of them were debonded inclusions. Also, for the butterflies, 80% of the inclusions were debonded. Moreover, almost all the cracked inclusions were debonded inclusions. For the cracked inclusions, 21% of the inclusions initiated micro-cracks and 50% of the inclusions resulted in butterflies. These statistics highlights the role of inclusion debonding in sub-surface damage initiation.

The characteristics of each catalogued inclusion included: length, width, inclination angle and depth from the surface. The measurements were made according to the definition given in Figure 5. The first observation was that inclusions initiated damage were bigger in size, length and width than that the inclusions not initiated damage. In Figure 14, the characterization of micro-cracks initiated by inclusion and butterflies are presented separately in order to investigate the characteristics of the inclusions that initiated them. In Figure 14 (b), the definitions of right and left wings relative to the ORD are shown in Figure 5 which are also applied to the left and right cracks in Figure 14 (a). The common observations from the length of micro-cracks and butterfly wings initiated from inclusions were: a) They

were longer in the axial sections than that in the circumferential sections. b) In the axial sections, their length on both right and left sides were almost the same, while for the circumferential sections the length of micro-cracks was slightly longer on the right hand side than on the left hand side.

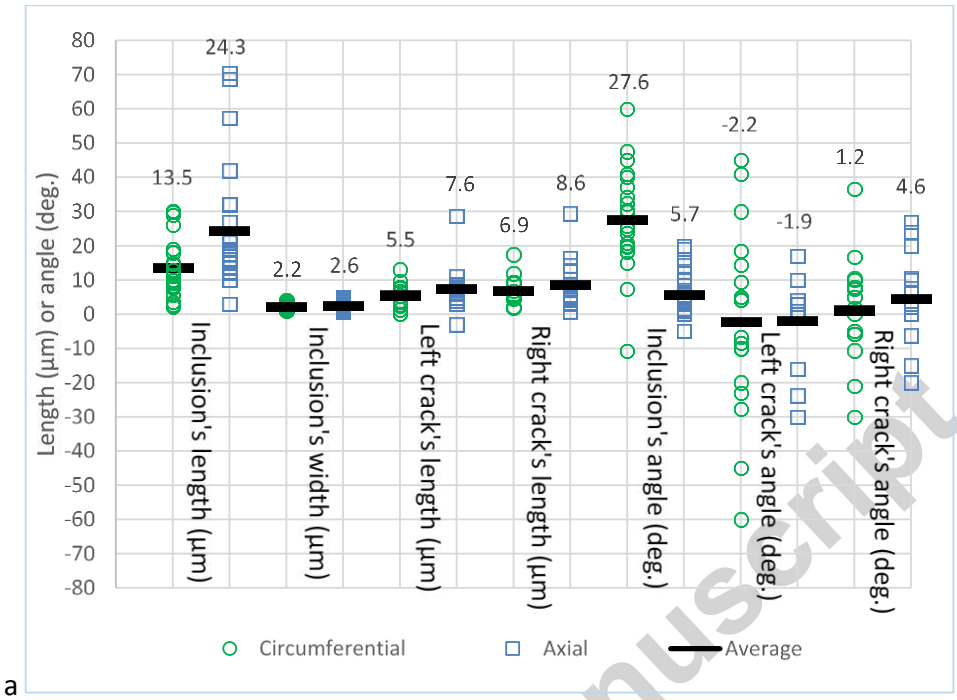


a

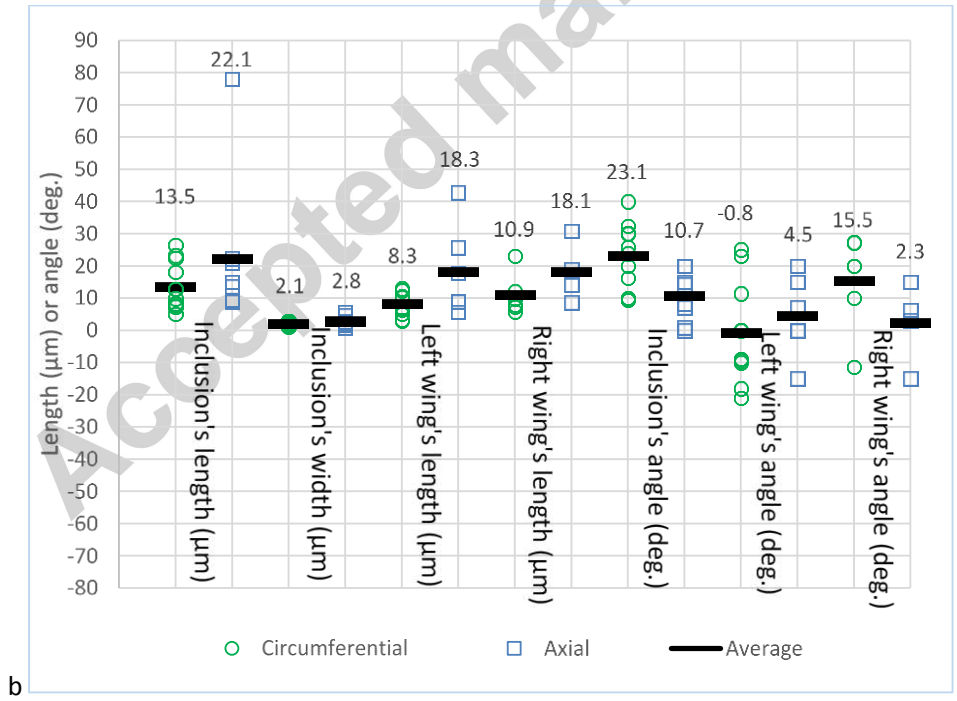


b

**Fig 14: Characterizations of subsurface damage (a) micro-cracks initiated by inclusions with their initiating inclusions (b) butterflies' wings with their initiating inclusions (the number above each characteristic feature refers to the average value)**

One of the main differences observed was that the butterfly wings were longer than micro-cracks in both of the circumferential and axial sections. The most recognisable feature regarding the angles of the micro-cracks and butterfly wings as shown in Figures 14, was the positive and bigger angle of the butterfly wings on the right side in the circumferential sections. This may be compared with micro-cracks on the same side, and sectioning direction which had shallow angles varied between positive and negative values. The small average angles of the micro-cracks in axial and circumferential sections were due to the fact that the angle values varied between positive and negative values at almost the same absolute value. However, the range of angles for the micro-cracks and butterfly wings was lower than 45˚ and this was the angle for the maximum principal shear stress $\tau_{1(max)}$. The angle and depth of $\tau_{1(max)}$ can be changed due to the effects of surface traction, which could be the reason for the observations of the angles for the butterflies and the cracks in Figure 14. The effects of inclusion depth and the relationships with the load on the surface will be discussed further in Section 6.

No clear relationship could be found between the size of the inclusions and the length of butterfly wings or micro-cracks initiated from inclusions. However, it was found that the total length of the inclusions and their associated cracks or butterfly wings showed a clear and direct relationship with inclusion length regardless of their depth as shown in Figures 15 (a) to (d), where the length of butterfly wings and micro-cracks on both the left and right side of the inclusions were measured. Accordingly, if the inclusion was considered as a weakening point of similar effect as a sub-surface micro-crack, the trend lines shown in Figures 15 (a) to (d) demonstrated that greater damage were created from bigger inclusions. These results, specifically those in Figures 15 (a) and (b), are in agreement with the expectation stated in the cleanliness standards such as ASTM E2283 [33] that the biggest inclusion is the most important for damage initiation. In the same context, Murakami derived relationships to describe the effect of inclusion size ($\sqrt{Area}$), on the fatigue limit of bearing steel, based on the assumption that a non-metallic inclusion acted like an initial crack length [34]. Although the number of butterflies found was less than that of the micro-cracks propagated from inclusions, the trend lines for the butterflies in Figure 15 (c) and (d) were similar to that of the micro-cracks in Figure 15 (a) and (b). Accordingly, the inclusion size affects butterflies and micro-cracks initiated from inclusions in the same way. Figures 15 (e) to (h) show that no consistent relationships can be recognized between the depth of butterflies or micro-cracks and the size of the initiating inclusions. Although Figure 15 (h) shows that inclusions causing butterflies are bigger when they are closer to the contact surface, the confidence in this trend is relatively low as can be seen from the $R^2$ value.

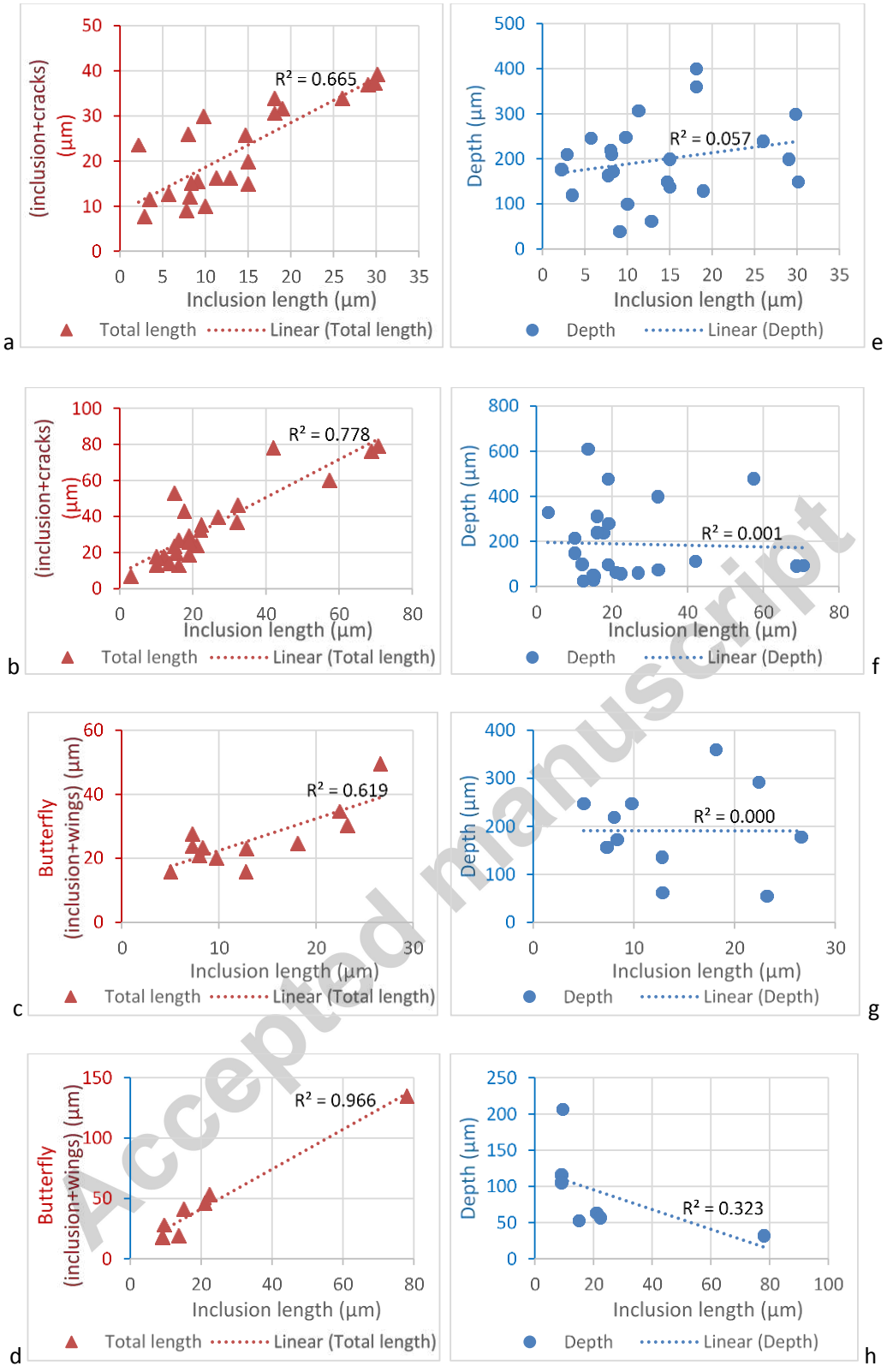




**Fig 15: Inclusion length vs total length with the depth of inclusions: (a) and (e) cracks initiated from inclusions in circumferential sections; (b) and (f) cracks initiated from inclusions in axial sections; (c) and (g) butterflies in circumferential sections; (d) and (h) butterflies in axial sections.**

## 6 Discussion of Surface Traction Effect on Sub-surface Initiated Damage

The sub-surface stress distribution, which, along with the stress risers (inclusions and voids) could be determinate in the initiation of sub-surface damage. For a rolling contact, the Hertzian contact pressure was used to calculate the sub-surface principal shear stress distribution $\tau_1$ according to the solutions of McEwen [35][36].

The load history of the examined bearing is unknown. However, the recommended maximum contact pressure $p_{max}$ for a wind turbine planetary bearing is 1500 MPa according to the standards BS EN 61400-4:2013 [37] or IEC 61400-4 [38] and this was assumed in the sub-surface stress calculations. Since the bearing had failed prematurely, an even greater value for the $p_{max}$ could be expected. Calculations were also made on the sub-surface stress distribution at higher contact pressure up to 2100 MPa. The depth of the maximum sub-surface shear stress $\tau_{1(max)}$ under $p_{max}$=1500 MPa was found to be 370 µm, which becomes deeper if under higher contact pressure. Figure 16 was created to show the percentage and frequency, of micro-cracks observed at each bin size of 50 µm of depth in this histogram. This figure shows that the occurrence of micro-cracks initiated from inclusion at a range of dominant depths, which is closer to the surface than the depth of $\tau_{1(max)}$ at various levels of contact pressure of 1500, 1700, 1800 and 2100 MPa. It is known that the location of the shear stress will be shifted towards the surface when surface traction occurs. If the maximum shear stress is considered to be the trigger for sub-surface damage, Figure 16 shows the observed damage initiated from inclusions at shallower depths that may have been affected by the occurrence of high surface traction. Under high surface traction, the location of $\tau_{1(max)}$ is shifted to the edge of the contact width and the value could be higher than that at the centre of the contact. The effect of surface traction could also be observed through the angles of the cracks and butterflies shown in Figure 14 which are not in line with the 45° of $\tau_{1(max)}$ under the centre of the contact when without surface traction. The additional stress due to surface traction or tensile stress, due to bearing seat waviness [17], could increase the stress concentration around the debonded inclusions and cause the WEA and WECs.

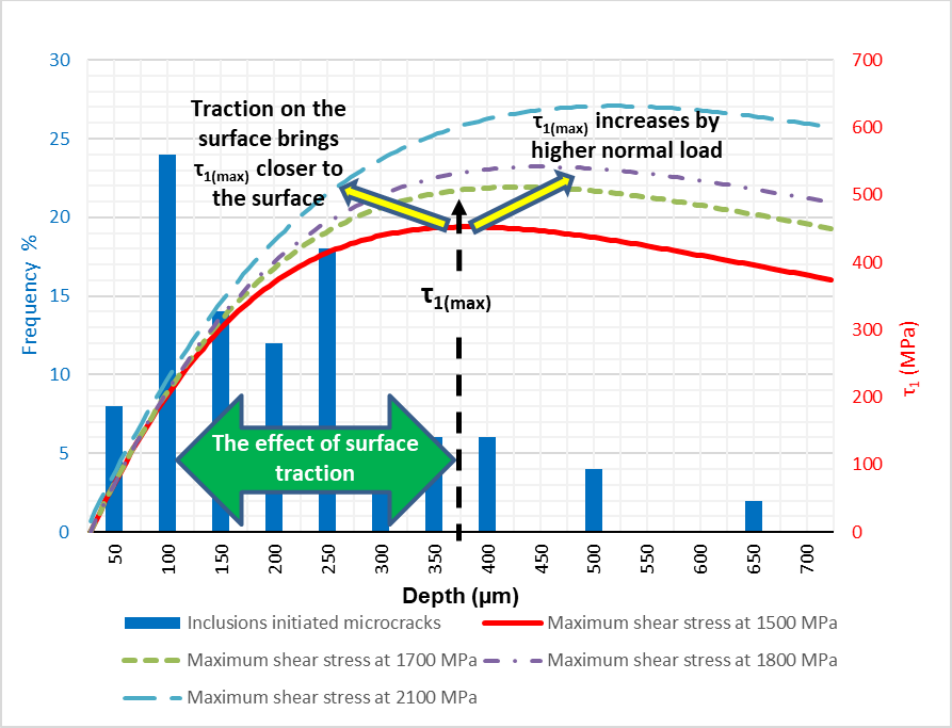


**Fig 16: Depth of micro-cracks in axial and circumferential sections compared with the depth of sub-surface maximum shear stress $\tau_{1(max)}$ at various levels of contact pressure**

Another investigation was conducted to determine the depth of the sub-surface material that was most affected by the surface loading. The sub-surface hardness variation was measured by the method described in Section 2. The variation in hardness could reflect hardening due to a higher load exceeding the material yield limit, and this could also be an indication for the location of sub-surface initiated damage. Measurements of this were carried out on a sample from the transfer region between the loaded and unloaded zones of the failed bearing, as shown in Figure 2. The average values and the standard deviation from three measurements at each depth are shown in Figure 17. In this figure, the loaded zone was under the raceway surface showing damage, and the unloaded zone was under the raceway surface that did not show damage, but was at the entrance to the loaded zone. Although both curves showed high hardness closer to the surface, the hardness for the loaded zone was higher at this depth close to the surface. If there was no surface traction the maximum hardness would be expected to be located around the depth of $\tau_{1(max)}$ which is 370 µm at 1500 MPa. Accordingly, this measurement could be another indication for the occurrence of surface traction because the maximum hardness measured was at the subsurface depth of less than 200 µm.

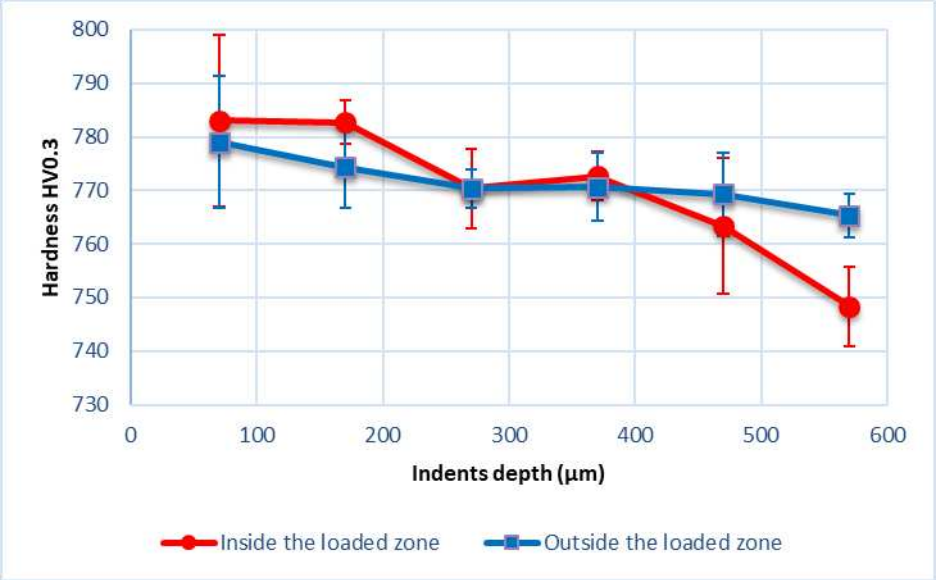


**Fig 17: Hardness variation with depth for the examined bearing**

## Conclusions

The focus of this study was to identify and analyse the inclusions initiated damage. The types of inclusions initiated damage were identified, including debonded inclusions, cracked inclusions, inclusion initiated micro-cracks, and Butterfly inclusions. The number of examined inclusions was 153 with some of them classified as more than one damage category. Accordingly, the total number of catalogued inclusions analysed was 208 which included both inclusions initiated damage and not initiated damage. The findings of this study are summarised as below.

1. Debondings between the WEAs and inclusion tips were observed in most of the butterflies found. Almost 60% of the debonded inclusions had cracks, initiated micro-cracks or formed butterflies. 52% of the inclusions that initiated micro-cracks were also deboned and 80% of the inclusions that formed butterflies were also debonded. Furthermore, almost all the cracked inclusions were also debonded. For the cracked inclusions, 21% of them initiated micro-cracks and 50% of them resulted in butterflies. These statistics highlighted the importance of debonded inclusion in sub-surface damage initiation.
2. The WEA in butterfly wings was found to be not as dense as the steel matrix according to the AFM scanning and looked like a damaged (discontinuous) material with lower hardness at the interface with the steel matrix. The observed damage topography could imply the occurrence of tensile or shear stress at the debonding gap between an inclusion and the steel matrix.
3. It was found that the total length of inclusion and butterflies or micro-cracks was directly proportional to the length of inclusions. Thus, a bigger inclusion was more detrimental to the lifetime of the bearings. Butterfly wings were found to be longer

and inclined with a higher angle than micro-cracks initiated by inclusions. Both butterfly wings and micro-cracks were longer in the axial direction.

4. By comparing the depth and inclination angle of the butterflies and the micro-cracks initiated from inclusions with the depth and angle of $\tau_{1(max)}$ calculated it revealed that high surface traction may have occurred. This conclusion was also supported by the measurement of subsurface hardness and the location of maximum hardness comparing to the depth of $\tau_{1(max)}$.

## Acknowledgement

The authors would like to acknowledge the support of an anonymous industrial partner for the provision of the failed bearing. The first author would like to thank the Iraqi Ministry of Higher Education and Scientific Research (http://www.igmohe.gov.iq/) and the University of Baghdad for sponsoring his PhD study.

## References

[1] M.-H. Evans, "White structure flaking (WSF) in wind turbine gearbox bearings: effects of 'butterflies' and white etching cracks (WECs)," *Mater. Sci. Technol.*, vol. 28, no. 1, pp. 3–22, Jan. 2012.

[2] a. Ruellan, F. Ville, X. Kleber, a. Arnaudon, and D. Girodin, "Understanding white etching cracks in rolling element bearings: The effect of hydrogen charging on the formation mechanisms," *Proc. Inst. Mech. Eng. Part J J. Eng. Tribol.*, vol. 228, no. 11, pp. 1252–1265, 2014.

[3] K. Stadler and A. Stubenrauch, "Premature bearing failures in industrial gearboxes," *Annu. Rev. Mater. Sci.*, vol. 9, no. 1, pp. 283–311, 2013.

[4] R. Wood, J. Basumatary, and M. Evans, "Energy-related tribo-corrosion research at the National Centre for Advanced Tribology at Southampton," *ASTM STP*, pp. 169–202, 2013.

[5] R. Errichello, R. Budny, and R. Eckert, "Investigations of Bearing Failures Associated with White Etching Areas (WEAs) in Wind Turbine Gearboxes," *Tribol. Trans.*, vol. 56, no. 6, pp. 1069–1076, Nov. 2013.

[6] B. Gould and A. Greco, "The Influence of Sliding and Contact Severity on the Generation of White Etching Cracks," *Tribol. Lett.*, vol. 60:29, no. 2, pp. 1–13, 2015.

[7] B. Gould and A. Greco, "Investigating the Process of White Etching Crack Initiation in Bearing Steel," *Tribol. Lett.*, vol. 62:26, no. 2, pp. 1–14, 2016.

[8] P. Rycerz, A. Olver, and A. Kadiric, "Propagation of surface initiated rolling contact fatigue cracks in bearing steel," *Int. J. Fatigue*, vol. 97, pp. 29–38, 2017.

[9] B. Gould, A. Greco, K. Stadler, E. Vegter, and X. Xiao, "Using advanced tomography techniques to investigate the development of White Etching Cracks in a prematurely failed field bearing," *Tribol. Int.*, vol. 116, pp. 362–370, 2017.

[10] J. Gegner, "Tribological Aspects of Rolling Bearing Failures," in *In: C.-H. Kuo (ed.), Tribology–Lubricants and Lubrication*, Rijeka, Croatia: InTech, 2011, pp. 33–94.

[11] T. Bruce, E. Rounding, H. Long, and R. Dwyer-Joyce, "Characterisation of white

etching crack damage in wind turbine gear-box bearings," *Wear*, vol. 338–339, pp. 164–177, 2015.

[12] A. Greco, "Bearing Reliability-White Etching Cracks (WEC)," in *Gearbox Reliability Collaborative Annual Meeting*, 2014.

[13] H. Uyama, "The mechanism of white structure flaking in rolling bearings," *Natl. Renew. energy Lab. Wind turbine*, pp. 1–37, 2011.

[14] H. Uyama, H. Yamada, H. Hidaka, and N. Mitamura, "The Effects of Hydrogen on Microstructural Change and Surface Originated Flaking in Rolling Contact Fatigue," *Tribol. Online*, vol. 6, no. 2, pp. 123–132, 2011.

[15] J. Gegner and W. Nierlich, "Tribology Seminar Wind Turbine A Recap Tribology Seminar," in *NREL Wind Turbine Tribology Seminar*, 2011.

[16] T. Bruce, H. Long, T. Slatter, and R. S. Dwyer-Joyce, "Formation of white etching cracks at manganese sulfide (MnS) inclusions in bearing steel due to hammering impact loading," *Wind Energy*, 2016.

[17] J. Lai and K. Stadler, "Investigation on the mechanisms of white etching crack (WEC) formation in rolling contact fatigue and identification of a root cause for bearing premature failure," *Wear*, vol. 364–365, pp. 244–256, 2016.

[18] A. M. Diederichs, S. Barteldes, A. Schwedt, J. Mayer, and W. Holweger, "Study of subsurface initiation mechanism for white etching crack formation," *Mater. Sci. Technol.*, vol. 32, no. 11, pp. 1170–1178, 2016.

[19] M. Brückner, J. Gegner, A. Grabulov, W. Nierlich, and J. Slycke, "Butterfly formation mechanisms in rolling contact fatigue," in *Proc VHCF-5*, 2011, pp. 101–106.

[20] M. H. Evans, A. D. Richardson, L. Wang, and R. J. K. Wood, "Serial sectioning investigation of butterfly and white etching crack (WEC) formation in wind turbine gearbox bearings," *Wear*, vol. 302, no. 1–2, pp. 1573–1582, 2013.

[21] J.-H. Kang, R. H. Vegter, and P. E. J. Rivera-Díaz-del-Castillo, "Rolling contact fatigue in martensitic 100Cr6: Subsurface hardening and crack formation," *Mater. Sci. Eng. A*, vol. 607, pp. 328–333, 2014.

[22] A. Warhadpande, F. Sadeghi, M. N. Kotzalas, and G. Doll, "Effects of plasticity on subsurface initiated spalling in rolling contact fatigue," *Int. J. Fatigue*, vol. 36, no. 1, pp. 80–95, 2012.

[23] A. M. Diederichs, A. Schwedt, J. Mayer, and T. Dreifert, "Electron microscopy analysis of structural changes within white etching areas," *Mater. Sci. Technol.*, no. 32:16, pp. 1683–1693, 2016.

[24] ASTM-E45-13, "Standard Test Methods for Determining the Inclusion Content of Steel," *Am. Soc. Test. Mater.*, pp. 1–19, 2013.

[25] M. N. K. and Tedric A. Harris, *Essential concepts of bearing technology*, 5th ed. Boca Raton, Fla. ; London: CRC/Taylor & Francis, 2007.

[26] L. E. Iorio and W. M. Garrison, "Effects of gettering sulfur as CrS or MnS on void generation behavior in ultra-high strength steel," *Scr. Mater.*, vol. 46, no. 12, pp. 863–868, 2002.

[27] C. Luo, "Evolution of voids close to an inclusion in hot deformation of metals," *Comput. Mater. Sci.*, vol. 21, no. 3, pp. 360–374, 2001.

[28] M. R. Allazadeh, C. I. Garcia, A. J. Deardo, and M. R. Lovell, "Analysis of Stress Concentration around Inclusions due to Thermally Induced Strain to the Steel Matrix," *STP49153S Quenching Cool. Residual Stress Distortion Control. STP49153S, L. Canale M. Narazaki, Ed., ASTM Int.*, vol. 6, no. 5, pp. 253–268, 2013.

[29] Y. Murakami, S. Kodama, and S. Konuma, "Quantitative-Evaluation of Effects of Non-Metallic Inclusions on Fatigue-Strength of High-Strength Steels .1: Basic Fatigue Mechanism and Evaluation of Correlation Between the Fatigue Fracture-Stress and the Size and Location of Non-Metallic Inclusions," *Int. J. Fatigue*, vol. 11, no. 5, pp. 291–298, 1989.

[30] P. W. D. and D. F. Pilkey, *Peterson's Stress Concentration Factors*. John Wiley & Sons, 2008.

[31] "International Organization for Standardization, BS EN ISO 6507-1: Metallic materials-Vickers hardness test part1: Test method," *BS EN ISO 6507-1*, 2005.

[32] V. Šmeļova, A. Schwedt, L. Wang, W. Holweger, and J. Mayer, "Microstructural changes in White Etching Cracks (WECs) and their relationship with those in Dark Etching Region (DER) and White Etching Bands (WEBs) due to Rolling Contact Fatigue (RCF)," *Int. J. Fatigue*, vol. 100, no. March, pp. 148–158, 2017.

[33] ASTM E2283, "Standard Practice for Extreme Value Analysis of Nonmetallic Inclusions in Steel and Other Microstructural Features," *Astm*, vol. 8, no. Reapproved 2014, pp. 1–11, 2015.

[34] Y. Murakami, *METAL FATIGUE: EFFECTS OF SMALL DEFECTS AND NONMETALLIC INCLUSIONS*, 1st ed. 2002.

[35] K. L. Johnson, *Contact mechanics*. Cambridge University Press, 1987.

[36] E. McEwen, "stresses in elastic cylinders in contact along a generatrix," *Philos. Mag.*, vol. 40, no. 454, 1949.

[37] BS-EN-61400-4, *Wind turbines Part 4: Design requirements for wind turbine gearboxes*. BSI Standards Publication, 2013.

[38] IEC-61400-4, *WIND TURBINES – Part 4: Design Requirements for Wind Turbine Gearboxes*. International Electrotechnical Commission, 2009.

**Highlights**

- Investigation of bearing subsurface damage initiation at non-metallic inclusion by the Atomic Force Microscopy and Nano-indentation hardness measurement.
- Debonding of non-metallic inclusions from the steel matrix caused the majority of subsurface damage including micro-cracks initiated by inclusions, WEA and inclusion internal cracking.
- A direct relationship was found between the size of inclusion and the total length of inclusion and butterfly wings or micro-cracks.
- Surface traction could be an important contribution to the subsurface damage initiation of the failed bearing.